Transient radiative transfer equation applied to oceanographic lidar

Kunal Mitra and James H. Churnside

We estimate the optical signal for an oceanographic lidar from the one-dimensional transient (time-dependent) radiative transfer equation using the discrete ordinates method. An oceanographic lidar directs a pulsed blue or green laser into the ocean and measures the time-dependent backscattered light. A large number of parameters affect the performance of such a system. Here the optical signal that is available to the receiver is calculated, rather than the receiver output, to reduce the number of parameters. The effects of albedo of a uniform water column are investigated. The effects of a school of fish in the water are also investigated for various school depths, thicknesses, and densities. The attenuation of a lidar signal is found to be greater than the diffuse attenuation coefficient at low albedo and close to it at higher albedo. The presence of fish in the water is found to have a significant effect on the signal at low to moderate albedo, but not at high albedo.

OCIS codes: 010.4450, 010.3640, 030.5620.

1. Introduction

Most of the research in radiative transfer in the ocean has been directed toward understanding the propagation of sunlight.[1] For these applications, the transient (time-dependent) term in the radiative transfer equation can be neglected. The justification for this assumption is that changes in the incident illumination are much slower than the changes imposed by the propagation of the light field through the medium. The assumption is satisfied clearly for solar illumination. However, lidar systems can use pulses that are shorter than the attenuation distance of seawater divided by the speed of light in water. Because of multiple scattering, light will be present at any given depth after the unscattered pulse has gone past. Understanding the lidar signal, therefore, requires a solution of the time-dependent radiative transfer equation.

Different numerical and approximate methodologies such as the Monte Carlo, spherical harmonics expansion, discrete ordinates, and the direct numerical integration technique are commonly used for steady-state radiative transport in the ocean.[1,2] The Monte Carlo method has proved to be an extremely powerful technique. It is well suited to use of empirical values for the properties of the medium. The errors in the results are unbiased and well understood, and implementation of this technique is relatively straightforward. However, it also has a couple of shortcomings. It tends to be computationally intensive—especially for lidar applications—because few of the initial photons contribute to the signal. In some cases, the relative importance of various processes is difficult to infer from a Monte Carlo calculation. The discrete ordinates method has also been used by researchers to analyze the steady-state radiative transfer in a coupled atmosphere–ocean system.[3]

Different techniques such as those used to solve the steady-state radiative transfer equation have been developed for the transient formulation in analyzing the lidar transport through scattering absorbing media. These include spherical harmonics expansion, discrete ordinates, and direct numerical integration. Some of this development has been stimulated by the problems of time-resolved optical tomography[4,5] of living tissues and organs using short laser pulses. This technology has the potential to provide physiological and morphological information to medical practitioners without some of the problems associated with harmful radiation, as in the case of x rays, or with harmful chemicals, as in the case of positron tomography and single-photon-emission tomography. Like seawater, biological tissue is a propagation medium that both scatters

and absorbs visible light. For the case of a short-pulse laser, the radiation signal of interest is the scattered intensity that persists for long periods because of multiple scattering after the initial pulse has been shut off. The advantage of performing transient analysis is the additional information about medium properties that is obtained from the measured signal.[6]

In this paper we consider the discrete ordinates solution to the transient radiative transfer equation in one dimension. A pulse shape that is typical of a Q-switched laser is used. Two general problems are treated. The first case corresponds to a uniform ocean with various scattering parameters. The Delta–Eddington distribution is used to approximate the scattering phase function of the seawater containing particles,[7] and the effects of different albedo are investigated. The approximation is based on measurements made with green light. Because penetration into the water column requires that a lidar use green or blue wavelengths, it is a reasonable approximation. According to the results of this model, it is demonstrated that the lidar attenuation coefficient is greater than the diffuse attenuation coefficient, although it can be less than the diffuse attenuation coefficient for high-albedo cases. This last result is not expected. At most, we calculated the lidar attenuation coefficient to be 2% less than the calculated diffuse attenuation coefficient, and this feature may not be present in a more sophisticated model. However, the effect is not a numerical artifact based on the current model, and there are preliminary reports of measurements that demonstrate the same effect.[8]

The second problem is one in which a discrete layer is present in the ocean having different optical properties. As an example, properties representative of a school of small fish are considered. The scattering properties of fish are assumed to be the same as diffuse spheres of an equivalent cross-sectional area. Aerial lidar is being considered for fish detection and for biomass surveys because of the difficulties and expenses encountered with more traditional surveying such as ichthyoplankton sampling, trawling, and acoustic surveying.[9,10] Aerial detection of fish has been demonstrated, and single-scattering and Monte Carlo models have been applied to analyze lidar performance.[2,11,12] In the tuna industry, improved techniques for locating schools of fish that are not associated with dolphins can reduce dolphin mortality during fishing operations. In epipelagic fisheries, such as those for anchovies, sardines, menhaden, and herring, the increasing costs of traditional ship-based survey techniques and the increasing requirements for accurate stock measurements are generating interest in lidar as a fisheries management tool. The results of our study show that fish can have a noticeable effect on the backscattered signal, depending on the number density of fish within a school, on its depth and thickness, and on the turbidity of the water.

2. Theoretical Development

The physical case under consideration is a one-dimensional scattering and absorbing layered ocean
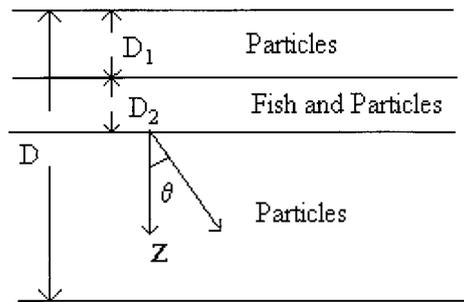
Fig. 1. Schematic of the problem under consideration.

medium with depth D, infinite horizontal extent, and azimuthal symmetry. As an example, fish layers having different properties from those of small particles (including mineral sediments, phytoplankton, and zooplankton) are present in the ocean between a depth of D_1 and $D_1 + D_2$ from the ocean surface (see Fig. 1). For simplicity, the boundaries of the medium are considered to be nonreflecting and nonrefracting. This geometry is the simplest possible and therefore is chosen to examine the effects of various approximations with the least additional mathematical complexity. The radiative transfer equation in this geometry, assuming azimuthal symmetry and constant properties, is written as[13]

$$\frac{1}{c}\frac{\partial L(z, \mu, t)}{\partial t} + \mu \frac{\partial L(z, \mu, t)}{\partial z} = -k_e L(z, \mu, t)$$

$$+ \frac{k_s}{2}\int_{-1}^{1} L(z, \mu', t)p(\mu' \rightarrow \mu)\mathrm{d}\mu' + S(z, \mu, t), \quad (1)$$

where L is the intensity (Wm^{-2} sr^{-1}), c is the speed of light in the medium, z is the Cartesian distance, t is the time, k_e is the extinction coefficient, k_s is the scattering coefficient, μ is the cosine of θ where θ is the polar angle measured from the positive z axis (positive being the direction of laser propagation, see Fig. 1), and p is the scattering phase function. Equation (1) is an integrodifferential equation in which the partial differentials represent a hyperbolic form of the equation. The scattering phase function, similar to that given in the literature,[1] satisfies the normalization

$$\frac{1}{2}\int_{0}^{\pi} p(\theta)\sin \theta \, \mathrm{d} \theta = 1. \quad (2)$$

The phase function in general can be represented in terms of a series of Legendre polynomials P_m as[14]

$$p(\Theta) = \sum_{m=0}^{M} a_m P_m(\cos \Theta), \quad (3a)$$

where Θ is the scattering angle, M is the order of anisotropy, and a_m are the coefficients in the expansion. The advantage of this formulation is that, for the one-dimensional plane-parallel geometry and azi-
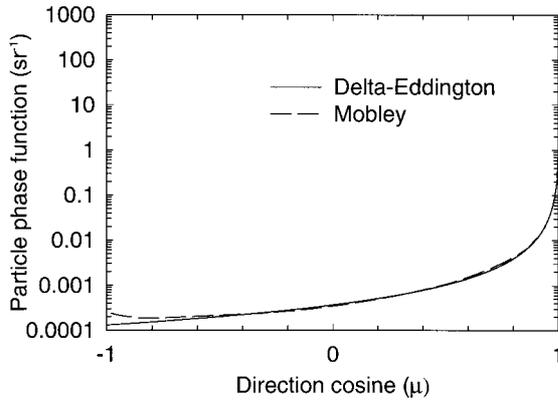
Fig. 2. Comparison of the phase function obtained by Mobley to its Delta–Eddington approximation.

muthal symmetry, the phase function depends on only the initial and final values of the polar angle, as[15]

$$\frac{1}{2\pi} \int_0^{2\pi} P_m(\cos \Theta) \mathrm{d}\psi = P_m(\mu') P_m(\mu),$$

$$\cos \Theta = \mu\mu' + \sqrt{1 - \mu^2} \sqrt{1 - \mu'^2} \cos(\psi - \psi'), \quad (3b)$$

where ψ is the azimuthal angle.

The phase function for particulates that are present in the ocean has been approximated by the Delta–Eddington approximation as[15]

$$p_p(\Theta) = 2f\delta(1 - \cos \Theta) + (1 - f)p^*(\Theta), \quad (4a)$$

or equivalently

$$p_p(\mu', \phi' \rightarrow \mu, \phi) = 2f\delta(\mu - \mu')\delta(\phi - \phi')$$
$$+ (1 - f)p^*(\mu', \phi' \rightarrow \mu, \phi), \quad (4b)$$

where f is the forward-scattering fraction of the unscattered intensity, δ is the Dirac delta function, and p^* is the new approximate smooth phase function that describes the scattered intensity and satisfies the relation

$$\frac{1}{2} \int_0^\pi p^*(\theta) \sin \theta \, \mathrm{d}\theta = 1. \quad (4c)$$

Figure 2 shows the comparison between the phase function obtained by Eq. (4) and developed by Mobley.[7] This function is an average of three measurements made at a wavelength of 514 nm in the San Diego, California, harbor; the water component is subtracted to obtain a typical particle function. Petzold's measurements, reported in Ref. 7, show that the phase functions of different waters are remarkably similar in shape, if not in absolute value, for green light. For example, the ratio of backscatter to forward scatter (at 0.1 deg) is 1.8×10^{-6} for the Mobley particle phase function, 1.7×10^{-6} for the turbid harbor measurement reported, 1.1×10^{-6} for the coastal ocean case reported, and 4.1×10^{-6} for

the clear ocean, all after subtracting the seawater component. The differences between these phase functions are not significant for our purposes. From Fig. 2, we can see that the Delta–Eddington approximation agrees with that of the Mobley phase function to about the same level of approximation as when the Mobley function is used for different waters. Other forms of analytical expressions for phase functions of oceanic water can be found in the literature,[16,17] but the Delta–Eddington form of the phase function as given by Eqs. (4) is used here for a relatively simpler numerical implementation and solution of Eq. (1). Generally, this function tends to underestimate the backscatter of various waters, especially of clear ocean water. Phase functions have been measured in coastal ocean and in clear ocean cases and could have been used here. However, the differences are expected to be small compared with the effects of different albedos, and we use a single function in all cases for numerical simplicity.

For the case of fish, the phase function can be represented adequately by Eq. (3a). The coefficients a_m are calculated as given by Ref. 18 using the phase function distribution for large diffusing spheres derived from geometric optics theory[15]:

$$p_f(\theta) = \frac{8}{3\pi} (\sin \Theta - \Theta \cos \Theta). \quad (5)$$

Clearly, fish are not large diffusing spheres. They are longer than they are wide, which will introduce an azimuthal dependence to the phase function. The skin is generally composed of discrete scales covered by a mucas layer and is probably not completely diffusing. The scattering is complicated further by the presence of flat structures, such as fins and a tail. We know of no measurements of the full phase function of schools of fish, and therefore we must make some assumptions; the simplest representation is that of a large diffusing sphere. In the one-dimensional geometry, the phase function is averaged over the azimuthal angle, so there is no reason to choose an elongated geometry such as ellipsoid over a sphere. Lacking any specific information about scattering properties, it seems reasonable to assume that the scattering is diffuse on the average. We recognize that individual scattering components may be far from this. We use large diffusing spheres because the calculations are relatively simple and because there are no measurements to suggest any better model.

For analysis, the total phase function in the fish layer is given by[1]

$$p(\cos \Theta) = \frac{k_{sp}}{k_s} p_p(\Theta) + \frac{k_{sf}}{k_s} p_f(\Theta), \quad (6)$$

where k_{sp} and k_{sf} are the scattering coefficients of particles present in the water and in fish, respectively. Here k_s is the summation of the scattering coefficients of particles and fish.

In the traditional transient radiative transport equation, the first term on the left in Eq. (1) is ne-

glected because of the large value of c. The intensity L remains time dependent, but the time variation is introduced traditionally through only the time-dependent boundary conditions or the time-dependent source.

The equation of transfer [Eq. (1)] is complicated because of the integral on the right side corresponding to the inscattering gain term. To reduce the integral to a simpler form, different approximations such as the spherical harmonics expansion, the discrete ordinates method, and the direct numerical integration technique were used. But it was found during computation that the spherical harmonics method yielded unrealistic results for the individual components of the intensity in any particular direction (for example, the direct backscatter component for the lidar), but was quite accurate for prediction of the integrated values of the intensity over all backscattered directions. Because in a lidar one is interested in the backscatter component $\theta = \pi$, the spherical harmonics method is not used for analysis of this problem. Direct numerical integration is found to be expensive from a computational point of view compared with the discrete ordinates method because of the higher number of angular directional nodes required to obtain the correct solution. The discrete ordinates method is based on a weighted, nonuniform discrete representation of the directional variation of the radiation intensity; therefore accurate solutions are obtained using fewer angular directional nodes. Therefore the focus in this paper is on the discrete ordinates method of solving the transient radiative transfer equation.

The method of discrete ordinates replaces the integral in Eq. (1) by a quadrature, such as Gaussian, Lobatto, or Chebyshev.[19,20] If μ_i's are the quadrature points between the limits of integration, -1 to 1, corresponding to a $2K$-order quadrature, and w_i's are the corresponding weights, Eq. (1) is reduced to the following system of coupled hyperbolic partial differential equations:

$$\frac{1}{c}\frac{\partial L_i(z, t)}{\partial t} + \mu_i \frac{\partial L_i(z, t)}{\partial z} = -k_e L_i(z, t)$$
$$+ \frac{k_s}{2}\sum_{j=-K}^{K} w_j L_j(z, t) p(\mu_j \to \mu_i) + S(z, \mu_i, t), \quad i, j \neq 0,$$
$$(7)$$

where $L_i(z, t) = L(z, \mu_i, t)$. The Lobatto quadrature of even order is used to avoid the value $\mu = 0$. The hyperbolic wave speed along the z direction of L_i corresponding to the discrete ordinate μ_i has the magnitude of $\mu_i c$.

A. Source Pulse and Boundary Conditions

The propagating pulsed source considered in this study is a pulsed laser with a fast rise and an exponentially decaying tail, which is typical of a Q-switched laser. The intensity in the medium can be separated into a collimated component, corresponding to the incident source, and a scattered intensity. If the colli-

mated intensity is L_c then L is the remaining part that can be described by Eq. (1). The collimated component of the intensity L_c for the case of nadir beam entry is represented by

$$L_c(z, \mu, t) = L_{\text{incident}} \exp(-k_e z)(t - z/c)\exp$$
$$\times [-(t - z/c)/\tau]H(t - z/c)\delta(\mu - 1),$$
$$(8a)$$

where L_{incident} is the peak power at the surface, $H(t)$ is the Heaviside step function, and τ is defined as 0.408 times the pulse-width at half-maximum. In this paper the pulse-width at half-maximum is equal to 10 ns, so $\tau = 4.08$ ns.

The source function S for the scattered intensity field is then given by

$$S(z, \mu, t) = \frac{k_s}{2}\int_{-1}^{1} L_c(z, \mu', t) p(\mu' \to \mu)\mu'. \quad (8b)$$

The boundary conditions are such that the intensities pointing inward at $z = 0$ and $z = D$ are zero, yielding

$$L(z = 0, \mu > 0, t) = L(z = D, \mu < 0, t) = 0. \quad (9)$$

The intensities at the interfaces $z = D_1$ and $z = D_2$ are assumed to be continuous.

B. Optical Properties of Fish

The scattering and absorbing properties of fish are calculated using the following relations:

$$k_{sf} = 2RAN, \quad (10a)$$
$$k_{af} = 2(1 - R)AN, \quad (10b)$$

where A is the cross-sectional area, N is the school density, and R is the reflectivity. In this analysis we used $R = 6.5\%$ and $A = 22.5$ cm^2, which are typical of 15-cm-long sardines.[10] The number density is varied from 3 to 100 cm^{-3}. The reflectivity of the unpolarized light R is calculated from the measurements of copolarized and cross-polarized values.[10]

The optical properties of the water depend on the type of ocean water used. For this analysis various types of ocean water ranging from clear water (lower albedo) to turbid water (high albedo) are considered.[7]

3. Results and Discussion

The numerical solutions for the discrete ordinates method are obtained with the subroutine PDECOL.[21] For all simulations, the grid sizes for both time and space variables are varied by one order in either direction from the used values, and the results are found to be stable and converging.

The results and discussion are divided broadly into two categories. First, the effects of the various types of ocean water on the lidar signal are investigated. The other aspect of the research deals with the effects on the signals of the presence of schools of fish having different number density, location, and width. The actual measured lidar signal will depend on a large number of factors, including aircraft altitude, telescope
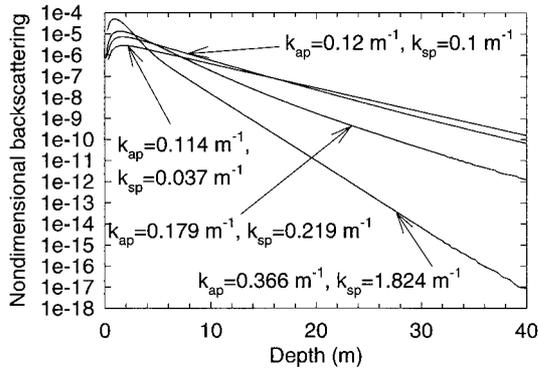
Fig. 3. Comparison of the backscattered signal as a function of depth for various types of ocean water using the discrete ordinates method.

diameter, optical filter characteristics, receiver field of view, detector characteristics, electronics bandwidth, background light levels, electronic noise, and the radiance of the laser light in the backscattered direction (i.e., $\mu = -1$) at the surface. To investigate the effects of various water types and fish, we use this radiance to represent the signal. The actual signal out of a lidar receiver can be calculated from these values, within the limits of the one-dimensional model used here.

First we consider the simulated backscattered signal for the case of ocean water containing no fish. Twelve discrete ordinates are used; increasing this number increased the computation time without a significant increase in numerical accuracy. As is usual in lidar, elapsed time is converted to depth using the speed of light in water. This is not strictly valid in highly multiple-scattering conditions, in which the path traveled by a photon can be greater than its depth. Thus the effective scattering depth at any particular time can be less than the depth used in the figures. The lidar signal is assumed to be proportional to the solution at $\mu = -1$, which is the most backward direction of the Lobatto quadrature. In reality, the lidar will receive light from any angle within its field of view. However, the returned light is not sharply peaked in the backward direction, and this is a reasonable approximation. The field of view also introduces an error in the time to depth conversion. For example, a lidar with a field of view of 100 mrad at an altitude of 300 m will receive light up to 50 mrad off nadir, which

travels 37 cm farther than light from nadir, with a delay of approximately 1 ns relative to the on-axis light. For our purposes, all these effects can be neglected.

A. Effect of Various Types of Ocean Water on the Measured Signal

Figure 3 represents the comparison of the backscattered signal at $\mu = -1$ for various types of ocean water, ranging from lower to higher optical albedo, but all using the same phase function. The four different types of ocean water considered have the following optical properties: (i) $k_{sp} = 0.037$ m^{-1}, $k_{ap} = 0.114$ m^{-1} ($\omega = 0.245$); (ii) $k_{sp} = 0.1$ m^{-1}, $k_{ap} = 0.12$ m^{-1} ($\omega = 0.454$); (iii) $k_{sp} = 0.219$ m^{-1}, $k_{ap} = 0.179$ m^{-1} ($\omega = 0.551$); (iv) $k_{sp} = 1.824$ m^{-1}, $k_{ap} = 0.366$ m^{-1} ($\omega = 0.833$). The varieties of water mentioned above represent a wide spectrum ranging from clear ocean to turbid harbor, as given in the literature.[7] The magnitude of the backscattered signal for higher albedo is higher than that of the lower albedo near the surface, but it drops more sharply with depth because the source pulse decays correspondingly faster for higher albedo. The slopes of the curves plotted in Fig. 3 yield the lidar attenuation coefficients (α) for the different types of ocean water and are given in Table 1. The lidar attenuation decreases with depth because of the increase of the angular distribution of the photons with depth.

The diffuse attenuation coefficient k_d is defined as the rate of change of downwelling intensity with depth.[22] For this calculation, the time-averaged forward-directed intensities are calculated at different depths for different types of water. The results of the diffuse attenuation coefficient obtained by time averaging of the transient model at each depth match the results obtained by the steady-state calculations. The diffuse attenuation coefficient also varies with depth but less significantly compared with the lidar attenuation coefficient. The value of k_d presented in Table 1 is calculated between a depth of 20–25 m. The diffuse attenuation coefficient $\hat{k}_d$ is also calculated on the basis of the quasi-single-scattering approximation.[23] This is represented as the sum of the absorption coefficient k_{ap} and the backscatter coefficient b_b obtained by integrating the volume-scattering phase function from $\mu = -1$ to 0. Thus $\hat{k}_d$ is an inherent optical property, and we might expect

Table 1. Optical Properties of Different Types of Water for Green Light

Albedo ω	Absorption Coefficient k_{ap} (m^{-1})	Beam Attenuation Coefficient $k_{ap} + k_{sp}$ (m^{-1})	Lidar Attenuation Coefficient 10–15 m α (m^{-1})	Lidar Attenuation Coefficient 20–25 m α (m^{-1})	Diffuse Attenuation Coefficient 20–25 m k_d (m^{-1})	Quasi-Single-Scattering Diffuse Attenuation Coefficient $\hat{k}_d$ (m^{-1})
0.245	0.114	0.151	0.133	0.131	0.116	0.134
0.454	0.120	0.220	0.163	0.159	0.124	0.170
0.551	0.179	0.398	0.246	0.218	0.183	0.288
0.833	0.366	2.190	0.377	0.367	0.374	1.277
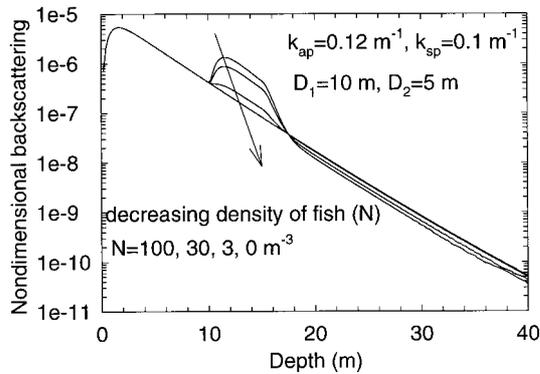
Fig. 4. Comparison of the backscattered signal as a function of depth for different number density of fish using the discrete ordinates method.

some relationship between it and the lidar attenuation, which does not depend on the solar illumination. From Table 1, we can see that α and $\hat{k}_d$ do agree fairly well at low albedo. At higher albedo, however, α becomes closer to k_d, and, in fact, becomes slightly lower than k_d at the highest albedo used. It is lower by less than 2%, which is more than the numerical uncertainty, but could be within the uncertainty introduced by approximations in the model. Note also that $\hat{k}_d$ is a better approximation to k_d at lower albedo. At higher albedo, multiple scattering becomes more important (more photons survive multiple interactions), and a quasi-single-scattering calculation would be expected to be a poorer approximation.

B. Effects of Fish in the Ocean

The effects of number density, thickness of schools of fish, and distance of schools of fish from the ocean surface on the backscattered signal are analyzed in this subsection. The optical properties of the ocean water used are $k_{sp} = 0.1$ m^{-1} and $k_{ap} = 0.12$ m^{-1}; the school density of fish N is 30 m^{-3} unless otherwise specified.

In Fig. 4 the backscattered signal is plotted as a function of depth for different number densities N of fish. A school of fish thickness of 5 m, present at a
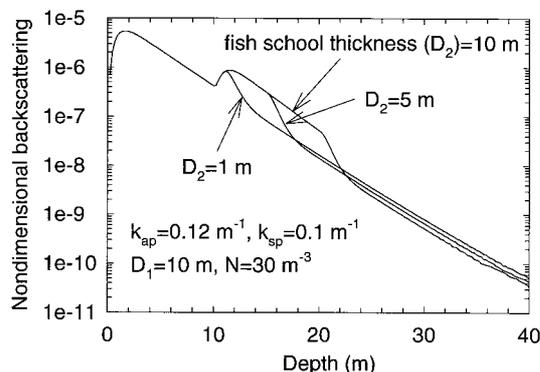
Fig. 5. Comparison of the backscattered signal as a function of depth for different thicknesses of schools of fish using the discrete ordinates method.
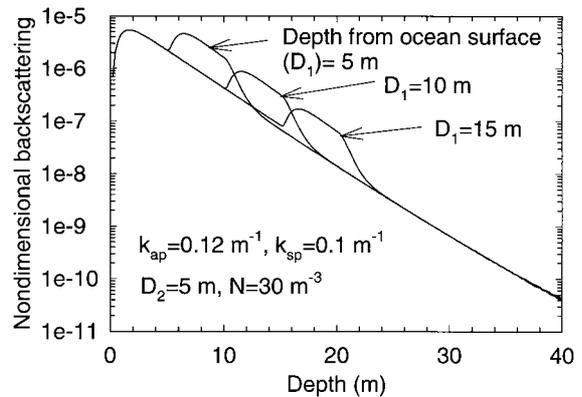
depth of 10 m from the ocean surface ($D_1 = 10$ m, $D_2 = 5$ m) is considered. The different values of N used are 3, 30, and 100 m^{-3}. The higher the value of N, the higher the scattering coefficient, as can be seen from Eqs. (10a) and (10b). Consequently, the magnitude of the backscattered signal increases because of the increased scattering events. But at the same time, because of a higher value of attenuation coefficient for the higher value of N, the source pulse decays faster, and correspondingly the backscattered signal drops off rapidly. In Fig. 4, the plot of the backscattered signal from ocean water containing no fish ($N = 0$) is also shown. The measured signal remains the same as that of the no fish case until the signal reaches the school of fish.

Figure 5 shows the backscattered signal distribution for different widths of fish schools ($D_2 = 1$, 5, and 10 m). The smaller the school width, the less is the pulse spreading and magnitude of the signal. The nondimensional backscattered signal is plotted in Fig. 6 as a function of depth for different regions where schools of fish are present from the surface of the ocean D_1. In this case the values of D_1 used are 5, 10, and 15 m. The first significant change in signal is observed corresponding to the depth of the fish from the ocean's surface. The closer the fish to the surface, the faster the decay of the corresponding backscattered signal.

The calculations with fish are repeated for the turbid water case ($k_{sp} = 1.824$, $k_{ap} = 0.366$). For these cases, no noticeable change between the curves with fish and without fish are observed. This suggests that detection of fish in highly turbid water would be difficult.

4. Conclusions

The present study is the first in the literature, to our knowledge, to detect a school of fish using transient radiative transfer formulation for signals obtained from oceanographic lidar. The significance of this comprehensive study examining the theoretical and numerical modeling of the transient radiative transport through ocean water is its implications for effective management and control of fisheries. This study

Fig. 6. Comparison of the backscattered signal as a function of depth for different depths from the ocean surface where schools of fish are present using the discrete ordinates method.

highlights the fact that the lidar attenuation coefficient is greater than the diffuse attenuation coefficient except for high-albedo water. The findings will prove to be a valuable tool for efficient analysis of lidar operation.

This research contains a number of limitations, approximations, and assumptions. These include the limitation of the one-dimensional geometry, simplified representations of both particulate and fish phase functions, the approximation that depth can be inferred directly from the time delay and the speed of light in water without taking multiple scattering into account, the assumption that surface effects can be neglected, and the assumption that the radiance at the surface can be used to infer lidar performance. This last assumption implies that we can design a lidar with low-noise and high-background rejection so that the features that we see in the calculations would actually be measured. Further research is being conducted into each of these areas.

Appendix A: Nomenclature

A Cross-sectional area of fish,
a_m terms in expansion of phase function,
c speed of light in the medium,
D depth of the medium,
f forward-scattering fraction,
h Heaviside step function,
k_a absorption coefficient,
k_d diffuse attenuation coefficient,
k_e extinction coefficient ($= k_a + k_s$),
k_s scattering coefficient,
L scattered radiation intensity,
L_c collimated component of intensity,
l fish length,
M degree of anisotropy,
N density of fish,
p scattering phase function,
P_m Legendre polynomials,
R fish reflectivity,
S source pulse,
t time,
z Cartesian coordinate,
α lidar attenuation coefficient,
μ $\cos \theta$,
θ polar angle measured from the positive x axis,
ψ azimuthal angle,
ω scattering albedo ($= k_s/k_e$),
Θ scattering angle.

References

1. C. D. Mobley, B. Gentili, H. Gordon, Z. Jin, G. Kattawar, A. Morel, P. Reinersman, K. Stamnes, and R. Stavn, "Comparison of numerical models for computing underwater light fields," Appl. Opt. **32,** 7484–7504 (1993).

2. M. M. Krekova, G. M. Krekov, I. V. Samokhvalov, and V. S. Shamanaev, "Numerical evaluation of possibilities of remote laser sensing of fish schools," Appl. Opt. **33,** 5715–5720 (1994).

3. Z. Jin and K. Stamnes, "Radiative transfer in nonuniformly refracting layered media: atmosphere-ocean system," Appl. Opt. **33,** 431–442 (1994).

4. A. Yodh and B. Chance, "Spectroscopy and imaging with diffusing light," Phys. Today **48,** 34–40 (1995).

5. Y. Yamada, "Light-tissue interaction and optical imaging in biomedicine," Ann. Rev. Fluid Mech. Heat Transfer **6,** 1–59 (1995).

6. S. Kumar, K. Mitra, and Y. Yamada, "Hyperbolic damped-wave models for transient light pulse propagation in scattering media," Appl. Opt. **35,** 3372–3378 (1996).

7. C. D. Mobley, "The optical properties of water," in *Handbook of Optics: Fundamentals, Techniques, Design* (Academic, San Diego, Calif., 1995), Vol. 1, Chap. 43.

8. J. H. Smart and K. H. Kwon, "Comparisons between *in situ* and remote sensing estimates of diffuse attenuation profiles," in *Laser Remote Sensing of Natural Waters: From Theory to Practice*, Proc. SPIE **2964,** 100–109 (1996).

9. J. H. Churnside and J. R. Hunter, "Laser remote sensing of epipelagic fishes," in *Laser Remote Sensing of Natural Waters: From Theory to Practice*, Proc. SPIE **2964,** 38–53 (1996).

10. J. H. Churnside, J. J. Wilson, and V. V. Tatarskii, "Lidar profiles of fish schools," Appl. Opt. **36,** 6011–6020 (1997).

11. J. L. Squire and H. Krumboltz, "Profiling pelagic fish schools using airborne optical lasers and other remote sensing techniques," Mar. Technol. Soc. J. **15,** 443–448 (1981).

12. D. L. Murphree, C. D. Taylor, and R. W. McClendon, "Mathematical modeling for the detection of fish by an airborne laser," AIAA J. **12,** 1686–1692 (1974).

13. R. Siegel and J. R. Howell, *Thermal Radiation Heat Transfer* (McGraw-Hill, New York, 1992).

14. G. E. Hunt, "The generation of angular distribution coefficients for radiation scattered by a spherical particle," J. Spectrosc. Radiat. Transfer **10,** 857–864 (1970).

15. M. F. Modest, *Radiative Heat Transfer* (McGraw-Hill, New York, 1993).

16. V. I. Haltrin, "Theoretical and empirical phase functions for Monte Carlo calculations of light scattering in seawater," in *Proceedings of the Fourth International Conference on Remote Sensing for Marine and Coastal Environments* (Environmental Research Institute of Michigan, Ann Arbor, Mich., 1997). Vol. 1, pp. I-509–I-518.

17. G. R. Fournier and J. L. Forand, "Analytic phase function for ocean water," in *Ocean Optics XII*, Proc. SPIE **2258,** 194–201 (1994).

18. E. Isaacson and H. B. Keller, *Analysis of Numerical Methods* (Wiley, New York, 1966).

19. M. P. Menguc and R. Viskanta, "Comparison of radiative transfer approximations for highly forward scattering planar medium," J. Quant. Spectrosc. Rad. Transfer **29,** 381–394 (1983).

20. S. Kumar, A. Majumdar, and C. L. Tien, "The differential-discrete-ordinate method for solutions of the equation of radiative transfer," J. Heat Transfer **112,** 424–429 (1990).

21. N. K. Madsen and R. F. Sincovec, "Algorithm 540 PDECOL, general collocation software for partial differential equations [D3]," ACM Trans. Math. Softwares **5,** 326–361 (1979).

22. C. D. Mobley, *Light and Water: Radiative Transfer in Natural Waters*, (Academic, New York, 1994).

23. H. R. Gordon, "Sensitivity of radiative transfer to small-angle scattering in the ocean: quantitative assessment," Appl. Opt. **32,** 7505–7511 (1993).